IWJ International Wound Journal

International Wound Journal ISSN 1742-4801

ORIGINAL ARTICLE

Changes in the extracellular matrix surrounding human chronic wounds revealed by 2-photon imaging

Jessica ES Sutcliffe[1], Christopher Thrasivoulou[1], Thomas E Serena[2], Leigh Madden[3], Toby Richards[4], Anthony RJ Phillips[5] & David L Becker[3,6]

1 Department of Cell and Developmental Biology, University College, London, UK
2 SerenaGroup, Wound and Hyperbaric Centers, Cambridge, MA USA
3 Lee Kong Chian School of Medicine, Nanyang Technological University, Singapore
4 Department of Surgery, University College London, London, UK
5 School of Biological Sciences, Auckland University, Auckland, New Zealand
6 Institute of Medical Biology, A*Star, Immunos, Singapore

Key words
Chronic wounds; Extracellular matrix; Second harmonic imaging

Correspondence to
DL Becker, PhD
Lee Kong Chian School of Medicine
Nanyang Technological University
11 Mandalay Road
Singapore 308232
E-mail: david.becker@ntu.edu.sg

doi: 10.1111/iwj.12789

Sutcliffe JES, Thrasivoulou C, Serena TE, Madden L, Richards T, Phillips ARJ, Becker DL. Changes in the extracellular matrix surrounding human chronic wounds revealed by 2-photon imaging. Int Wound J 2017; 14:1225–1236

Abstract

Chronic wounds are a growing problem worldwide with no effective therapeutic treatments available. Our objective was to understand the composition of the dermal tissue surrounding venous leg ulcers and diabetic foot ulcers (DFU). We used novel 2-photon imaging techniques alongside classical histology to examine biopsies from the edges of two common types of chronic wound, venous leg ulcers and DFU. Compared to normal intact skin, we found that collagen levels are significantly reduced throughout the dermis of venous leg ulcer biopsies and DFU, with a reduction in both fibril thickness and abundance. Both wound types showed a significant reduction in elastin in the upper dermis, but in DFU, the loss was throughout the dermis. Loss of extracellular matrix correlated with high levels of CD68- and CD18-positive leukocytes. 2-photon imaging of the extracellular matrix in the intact tissue surrounding a chronic wound with a hand-held device may provide a useful clinical indicator on the healing progression or deterioration of these wounds.

Introduction

Normally, most skin lesions heal rapidly and without incident. The healing process comprises of an initial inflammatory reaction with an influx of neutrophils to attack any bacteria that may have invaded the wound, which is followed by macrophages to clean up the resulting cellular and bacterial debris (1). Wound-edge (WE) keratinocytes and fibroblasts then proliferate and migrate to close the wound, after filling the gap with granulation tissue and laying down new extracellular matrix (ECM). During this process, the initial pro-inflammatory response subsides, and the resulting new ECM of the scar is then remodelled over a period of months or years (2). However, in some members of the population, such as the elderly and the diabetic, this process can fail and chronic wounds can result (3,4). In these wounds, the pro-inflammatory response is never fully attenuated, and the wounds are thus constantly inflamed with the subsequent healing process incomplete (5). The reasons behind the lack of healing can vary but are often due to problems in the blood supply to the area of the lower limb. Chronic wounds are a growing and costly problem all over the world as the population grows older and the incidence of predisposing chronic states, such as diabetes, becomes epidemic (6). The quality of life for patients with chronic wounds is greatly compromised (7), as is their life expectancy in severe

Key Messages

- the degradation of the extracellular matrix spreads beyond the chronic wound bed into the wound-edge tissues, with different characteristics for venous leg ulcers and diabetic foot ulcers
- unstained collagen extracellular matrix can be imaged by 2-photon second harmonics
- this imaging approach may provide a new way to monitor the progression of a chronic wound

cases, which is reportedly reduced to as little as 5 years, a mortality that can be worse than many common cancers (8). For healthcare services, the costs are very high and growing rapidly, with estimates of over US$25 billion being spent each year in the USA (6). Unfortunately, no effective specific therapeutic treatments are currently available, particularly for diabetic ulcers, which can result in amputation of the lower limbs (3). Understanding the multiple factors that are at play in preventing the healing of these chronic wounds will help us identify new treatments.

Chronic wounds are characterised by excessive proteolytic activity from matrix metaloprotienases (MMPs) (9,10) such as elastase and plasmin (11), which can each have a negative effect on the structure of the dermal connective tissue. MMPs have been reported to exhibit elevated activity in chronic wound fluids, and their activity may spread beyond the wound bed (12). Their uncontrolled activity may interfere with the healing process as newly formed ECM in the granulation tissue will be prematurely broken down (13). The tissue environment surrounding the wound is also very important as this is the source of new cells to fill the defect and heal the wound. If the structure of the connective tissue of the surrounding dermis is degenerating, it will be unable to withstand the everyday stresses and strains placed upon the skin, and so, the wound is likely to get larger. Beyond this, the different MMPs have many roles in the wound-healing response in addition to degrading the ECM, and they have been shown to influence the immune response and activate growth factors (14), which can have positive and negative effects on healing. Indeed, attempts to attenuate protease activity in chronic wound fluids has been explored with some reported success (15–17).

Other theories have proposed that an unresolved inflammatory response will generate elevated levels of proteases and cytokines in the inflammasome, which has been suggested to contribute to matrix degradation and impaired healing (18). Others have suggested that the development of senescent fibroblasts around a chronic wound contribute to poor healing and an enhanced degradation of the ECM (19,20). It was estimated that if the number of senescent fibroblasts exceeded 15%, then healing would be compromised (21,22). Whilst determining the percentage of senescent cells would require a biopsy to be taken, another approach could be to image the extent of the damage by visualising the ECM degradation (22,23). The use of hand-held 2-photon imaging devices that are now available may be able to determine the extent of ECM degradation and in turn be able to provide an indication on the progression or regression of healing in chronic wounds.

Methods

Ethical approval

All chronic leg and foot wound and normal arm tissue was sourced in the USA (Western Institutional Review Board, 3535 Seventh Avenue, Olympia, WA 98502-5010), whilst control leg and toe tissue was obtained in the UK (National Research Ethic Service (NRES) Committee (11/0395) REC 11/LO/1483). A total of 19 Venous leg ulcers (VLU) subjects were evaluated, with an average age of 59 (31–79), 63% male with an average wound age of 6 months (1·5–108) and average size of 9·9 cm^2 (2–113). A total of 11 DFU patients were examined, with an average age of 59 (48–82), 64% male with an average wound age of 4 months (1–26) and average size of 6·6 cm^2 (0·56–22·2). Details of the individual patients in this study have been published previously (24).

Second harmonic generation (SHG) imaging

Tissue sections were defrosted, re-hydrated in distilled H_2O and temporally mounted using 50-mm glass coverslips prior to imaging. In some instances, the nuclei of sections were counterstained with Hoecsht to show where the epithelial layer was located. Image acquisition was performed on a Leica SP2 AOBS confocal multi-photon (MP) laser-scanning upright microscope (Leica, Milton Keynes, UK), equipped with a pulsed, mode-locked femtosecond (fs) Ti: Sapphire Tsunami laser synchronously pumped by a Millenia VII (Spectra-Physics, Mountain View, CA), diode-pumped, solid-state frequency-doubled laser capable of delivering up to 8·5 W pumping power at 532 nm.

All SHG image acquisition was performed at 840 nm, which has previously been found to be the optimum wavelength for collagen types I and III (25,26). The pulse width of the Tsunami was 80 fs with a pulse repetition rate of 80 Mhz. Laser power output at the microscope was recorded with a coherent power metre and calibrated for all samples to deliver peak power of $0{\cdot}4 \times 10^8$ W/cm^2 and was consistently maintained below the damage threshold of the samples, which – for collagen in sections – was found to be $1{\cdot}5 \times 10^8$ W/cm^2. An IST laser spectrum analyser coupled with a Tektronix TDS 210 oscilloscope was used to tune the laser to the desired wavelength. An electro-optical modulator (EOM) (Linos LIV20) received the laser output before delivery to the confocal microscope through a series of optical mirrors. The EOM allowed the laser intensity at the objective to be controlled and optimised. EOM was set at 90% for imaging to ensure that the polarisation of the incidental laser beam remained consistent across all specimens.

In order to image the complete section, we used a motorised stage (Mietzhouser, GmbH), controlled by the Leica software, to perform automated montages from multiple fields that were imaged with a ×25, 0·95 NA oil objective, ×1·7 zoom and 2 µm Z stack. The SHG signal in the backscattered geometry was captured in the de-scanned detector with the pinhole set to the maximum of 600 µm. The Leica microscope incorporates a programmable, prismatic beam splitter, which is capable of single- and multi-chromatic beam splitting. The backscattered photons are subsequently focused through the objective lens with an estimated beam diameter of 0·14 µm ($\lambda_p = 840$ nm) and delivered through the prismatic beam splitter, programmed to collect light at 410–430 nm before passing it on to the photomultiplier tube (PMT). The coherent SHG signal formed in the transmission geometry was detected by the transmission detector via the microscope condenser, with a 420-nm df 30 nm band pass filter inserted in the light path (Chroma Inc., Vermont, USA). At the end of image acquisition, the automatic montage software produced a final compilation image of the all fields.

Hoechst nuclear stain was imaged with a single-photon excitation at 351/364 nm laser, permitting the visualisation of the

nuclei and autofluorescence of collagen and elastin. Subsequently, lambda scans were performed on the same microscope fields with photon excitation at 840 nm. Emission spectra were collected between 400 and 700 nm at 10-nm bandwidth. Differentiation of the different ECM components and other photon autofluorescence elements of the sample was achieved using the inbuilt 'spectral unmixing' (SUM) algorithm of the Leica software to separate and subtract the SHG collagen signal from the autofluorescence signal. Images show SHG collagen signal (green backscatter and red forward transmission), elastin and nuclei (blue).

Herovici histological stain

Frozen sections were defrosted and immersed in distilled water to dissolve excess OCT and transferred to a Herovici staining solution [50 ml of van Gieson's solution (saturated picric acid (Sigma, Aldrich, UK – P6744) and 1% aqueous acid fuschin (Sigma-Aldrich, Poole, UK – 857408)), 50 ml of 0·05% aqueous methyl blue (Sigma-Aldrich, UK – M5528), 10 ml of glycerol (VWR, Leicester, UK – 444485B1) and 0·5 ml of saturated aqueous lithium carbonate (Sigma-Aldrich, UK – 62470) solution] for 2–3 minutes. The slides were then dipped into 1% acetic acid, followed by distilled water. The tissue was dehydrated through alcohol baths prior to clearing with xylene and mounting in DPX. Staining: collagen type III – blue; collagen type I – red/purple; epidermis – yellow.

Verhoeff van Gieson histological stain

The slides were placed in Verhoeff's staining solution [20 ml of 5% alcoholic haematoxylin (Sigma-Aldrich, UK – H31316), 5 ml of 10% ferric chloride (Sigma-Aldrich, UK – 157740), 8 ml of Weigert's iodine solution, 2% potassium iodide (Sigma-Aldrich, UK – P4286) and 1% iodine (Sigma-Aldrich, UK – 207772)] for 1 hour, washed in tap water and differentiated in 2% ferric chloride. The slides were washed in running tap water, counterstained with Van Gieson's (5 ml of 1 % aqueous acid fuschin and 100 ml of saturated picric acid) solution for 4 minutes and dehydrated through alcohol baths and then xylene prior to mounting. Staining: collagen – red/pink; elastic fibres and nuclei – black; other tissue; yellow.

Immunohistochemistry

All human tissue was stained using the VECTORSTAIN Elite ABC Universal R.T.U. kit. All primary antibody incubations occurred overnight at 4 °C, in a humid staining chamber; CD68 (Thermo-Scientific, Newport, UK – MS-397-P Rabbit polyclonal) 1:100 overnight, developed for 20 minutes and CD18, (AbD Serotec, Kidlington, UK – MCA503 Rabbit polyclonal) 1:200 overnight, developed for 15 minutes. All tissue was counterstained (nuclei) using methyl green.

Imaging

All slides stained via immunohistochemistry were montage-imaged using the ×20 objective in the brightfield mode on an AXIO Scan.Z1 slide scanner, (Zeiss, Cambridge, UK). The Hammamatsu NanoZoomer 2·0-RS slide scanner (Hammamatsu, Welwyn, UK) was used to montage-image all histological samples stained via the Verhoeff van Gieson (VvG) and Herovici techniques. A Leica DM2500 upright microscope fitted with a Leica DFC310FX camera was used to take ×20 images of Herovici, VvG and sections stained via immunohistochemistry.

Statistics

All statistical analyses were carried out in SPSS. The data were first tested for normality using the Kolmogorov–Smirnoff test, permitting parametric analysis. Data was then analysed using an ANOVA, followed by Dunnett's post-hoc test. Significance was considered at values $\leq 0{\cdot}05$.

Results

Examination of the collagen and elastin content of the ECM

Overall, the degree of signal emanating from two of the main ECM constituents, collagen and elastin, were diminished in samples from both ulcer aetiologies compared to the control arm and the leg skin (Figure 1A). It was unclear whether the reduced signal was due to a decrease in collagen and/or elastin, so a combination of SHG and conventional imaging was used, alongside traditional histological techniques comprising VvG and Herovici stains, to investigate this. Separation of the SHG signal from the collagen and the autofluorescence from all of the ECM components was achieved via SUM. This was performed following an 840-nm MP laser lambda scan to obtain the spectra for collagen and then a UV-stimulated lambda scan to obtain the autofluorescence spectrum of all ECM fibres (Figure 1B). In non-wounded arm and leg tissue, the SHG collagen signals (green and red for forward and backscattered signal, respectively) were distinctly different between the papillary and reticular dermal architecture. Throughout the papillary dermis, a network of thin and fine collagen fibrils were seen (Figure 1C and 1E). In the deeper reticular zone, thick, fibrillar collagen bundles were interwoven to form a 'basket weave' pattern (Figure 1C and 1E). Less abundant than collagen, the autofluorescent, UV-stimulated elastin signal (blue) produced a similar pattern. Thin elastin fibrils were solely detected in the papillary dermis, whilst thick elastic fibres were seen throughout the reticular dermis, interspersed between collagen fibres (Figure 1C and 1D).

Verhoeff van Gieson

The VvG technique, staining collagen red and elastin black, was used to corroborate the distribution patterns identified via SHG and spectral imaging. Slight under-differentiation was aimed for to ensure that microfibril staining was not erroneously eliminated. One of the benefits of this technique over autofluorescence was the enhanced ability to detect the oxytalan and euylan microfibrils of the papillary dermis. Comparisons to the SHG/autofluorescence images confirmed that the quantified elastin results represented the true distribution. Fine

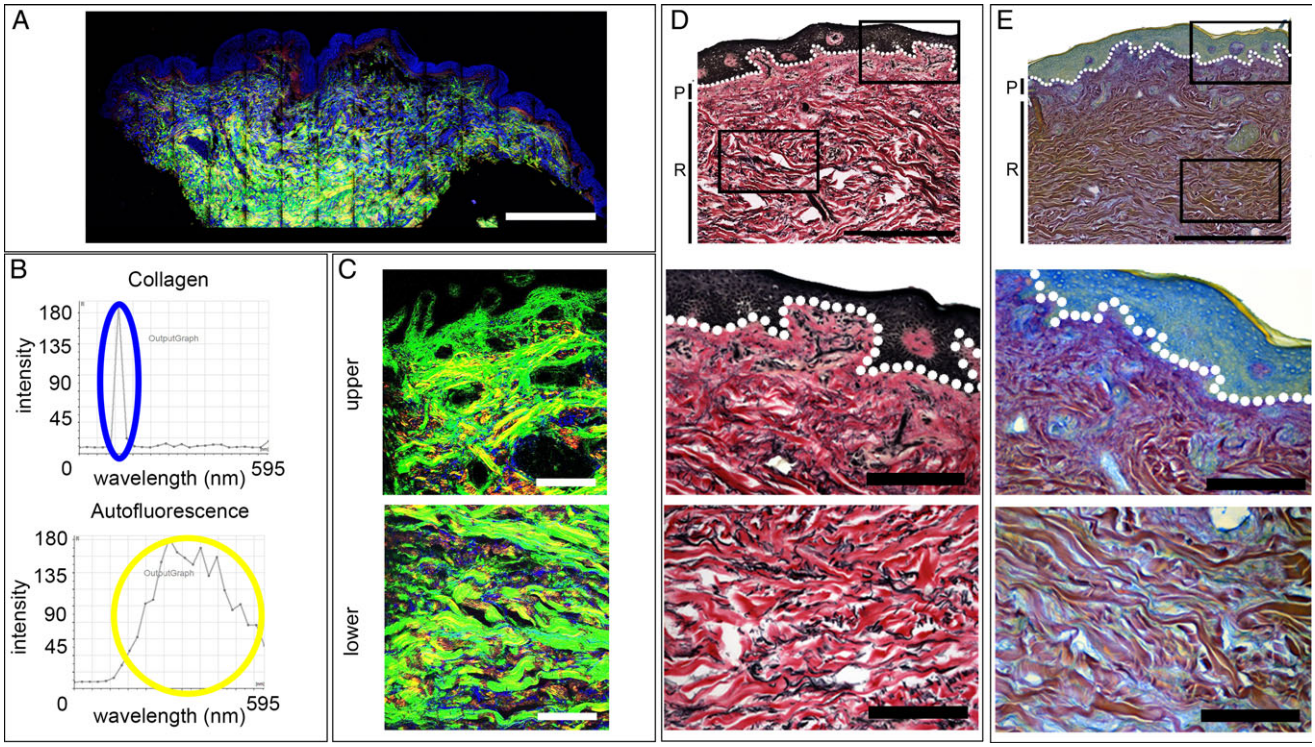

Figure 1 2-photon imaging of the extracellular matrix of normal arm and leg skin. (A) Second harmonic generation imaging of collagen (green, backscatter; red, forward detection) and autofluorescence imaging and elastin fibres and nuclei (blue) in normal arm and leg skin. (A) Montage of a 4-mm biopsy of arm skin. (B) Lambda scans of the SHG of collagen signal and autofluorescence of elastin. (C) High-power images of upper and lower dermis from leg skin. (D) Normal arm skin with Verhoeff van Gieson (VvG) staining collagen red and elastin black. Montage followed by high-power images of the upper, lower and deep dermis. (E) Normal arm skin with Herovici staining differentiating between collagen type I, stained purple, and type III, blue. Scale bars A, 1 mm; C, D and E, 1 mm and 200 μm.

elastin microfibrils (oxytalan) were seen in the papillary layer (Figure 1D) forming branching, 'candelabra-like' structures. Thick black elastic fibres were seen throughout the reticular dermis. The rich, red staining further highlighted the presence of thick reticular collagen fibres (Figure 1D).

Herovici histological stain

Herovici staining can differentiate between collagen type I, stained purple, and type III, blue (although caution must be applied as the stain colours are not always definitive). Thin type III collagen fibrils were seen in the papillary dermis as light blue staining (Figure 1E). Within the reticular dermis, thick collagen I rich bundles dominate, stained purple, interwoven between thin blue fibres.

Venous leg ulcers

A significant decrease in the dermal collagen content of between 40% and 48% was seen in VLUs compared to intact leg skin at all examined locations, upper ($P < 0{\cdot}05$), lower ($P < 0{\cdot}001$) and deep ($P < 0{\cdot}05$) dermis (Figure 2). The reduction for elastin was 38–89% and restricted to the upper ($P < 0{\cdot}001$) and lower ($P < 0{\cdot}01$) regions. The upper dermis was dominated by the presence of fine collagen fibrils (Figure 2A and 2C). Although the structure and distribution of these were similar to the papillary dermis of intact skin, the basket weave organisation was missing, and the zone of fine fibrils was much larger than in the control skin, extending into the lower dermal region. Within the deeper dermal zone, the fibril thickness was moderately increased when compared to that of the upper dermis (Figure 2A and 2C). In addition, the average signal intensity within both the upper and lower areas was greatly diminished (Figure 2D). Whilst mature collagen bundles were seen in all deep dermal tissues, the fibres were slimmer than those seen in normal leg tissue. Overall, the signal from the collagen content at each examined location was significantly reduced (Figure 2D). A 40% ($P < 0{\cdot}05$) reduction of collagen in the upper dermis with 48% ($P < 0{\cdot}001$) decrease in the lower dermis was observed, whilst the mature collagen within the deep dermis had a lower loss of 35% ($P < 0{\cdot}05$).

Elastin was almost completely absent from the upper dermis (Figure 2A and 2B), with an 89% reduction in abundance (Figure 2D) compared to the same region of control skin ($P < 0{\cdot}001$). This is exemplified by the restriction of elastic fibres to the bottom fifth of the tissue sample, shown in Figures 2A and 2B. Although the severity of elastin loss was diminished in the lower dermis to 38%, with the presence of moderately thick elastic fibres throughout this region (Figure 2B), the overall elastin content was still significantly ($P = 0{\cdot}018$) reduced (Figure 2D). However, whilst there was

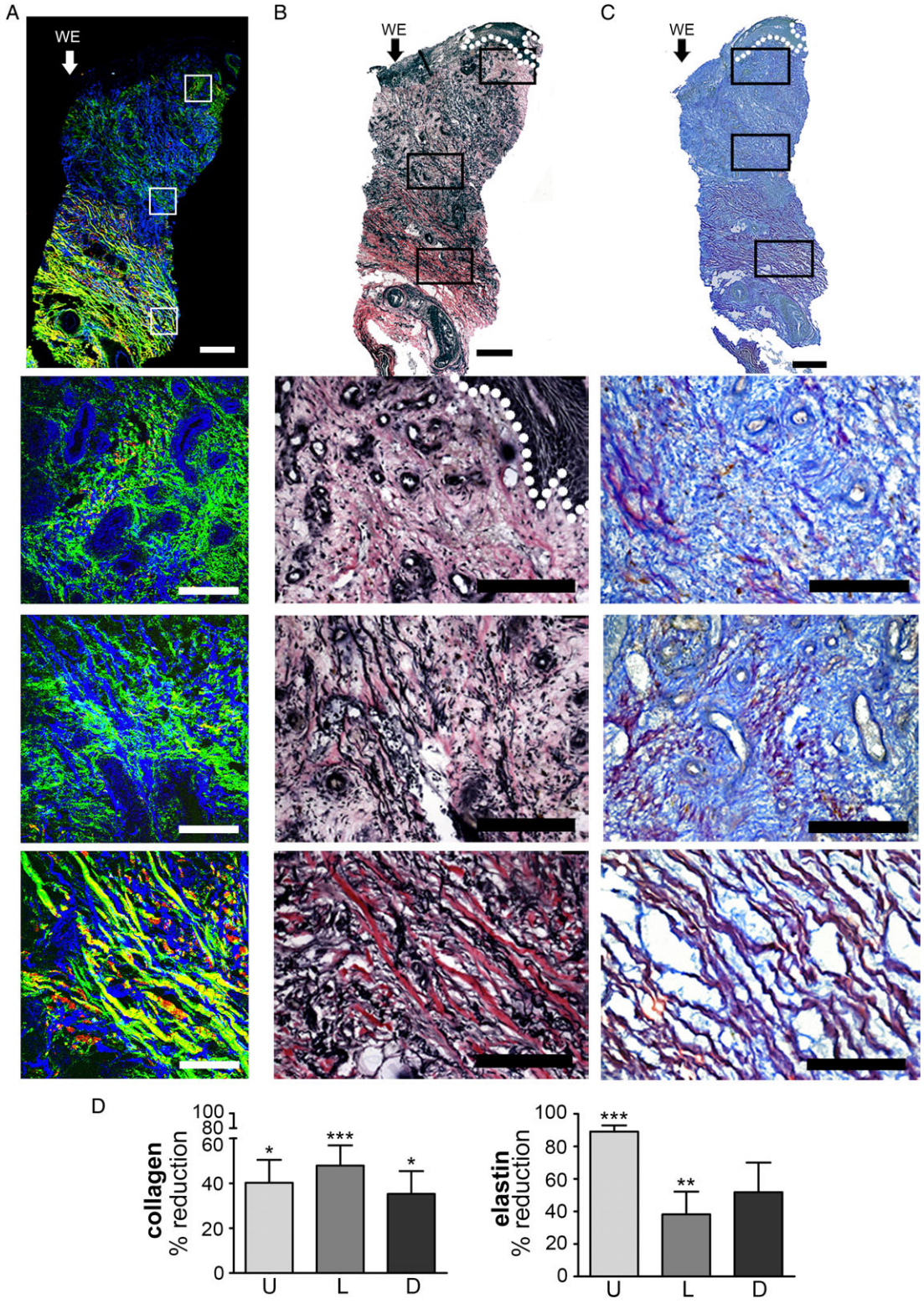

Figure 2 Imaging of the extracellular matrix of venous leg ulcer biopsies. (A) Second harmonic generation and autofluorescence imaging of collagen (green, backscatter; red, forward detection) and elastin fibres and nuclei (blue) in a venous leg ulcer biopsy. Montage of high-power SHG and autofluorescence images of a 4-mm skin biopsy from the edge of a venous leg ulcer. High-power images of the upper, middle and lower dermis. (B) Verhoeff van Gieson (VvG) staining collagen red and elastin black in a sister section. Montage followed by high-power images of the upper, middle and lower dermis. (C) Herovici staining differentiates between collagen type I, stained purple, and type III, blue. (D) Graphs quantifying SHG images and the % reduction in signal from collagen and elastin. Arrow and WE marks wound edge on the left side of the images. Error bars: mean ± SEM. Scale bars, montage 1 mm and high power 200 μm.

a reduction in elastin signal, no significant difference was detected in the deeper dermal region.

The VvG stain showed a zone of dermal elastin loss as a consistent feature of VLU biopsies (Figure 2B). The depth of the loss of dermal elastin ranged from 135 to 1000 μm. In the majority of samples, this extended from the visible wound edge (WE) to the far edge (FE) of each biopsy (Figure 2B). VvG collagen staining was diminished, compared to control dermal tissue, with a colour shift from red to pink. Richer, darker staining was only identified in regions of thick fibre aggregation (Figure 2B).

Herovici staining showed that the type I to type III ratio was disturbed in the majority of the 14 VLUs. There was marked increases in type III and corresponding decline in type I abundance (Figure 2C). Thin blue fibrils were clearly identified throughout the upper and lower dermal regions, intermingled with fine type I collagen strands, which increased in thickness with depth to deep dermal tissue (Figure 2D).

Taken together, these results show a distinct upper zone in the intact WE of VLU that lacks the normal distribution of robust ECM of both collagen and elastin bundles; instead, only very fine strands remained. However, in the deep reticular dermis, the normal distribution of thick bundles of collagen and elastin could still be detected.

Diabetic foot ulcers

The ECM of diabetic foot ulcers (DFUs) was dominated by fine collagen fibrils both within the upper and lower dermis (Figures 3A and 3C). In the majority of samples, there was an absence of the normal thick, mature collagen fibres. Instead, thin, elongated fibrils dominated both the upper and lower dermis, forming an irregular network, with no discernible consistent angle of orientation or basket weave appearance. The elastin content of DFUs was significantly ($P = 0{\cdot}045$) diminished by 80% in the upper dermis only (Figure 3D). Despite a reduction of approximately 50% of the elastin, significance was not met in the lower dermal tissue. Although the degree of elastin absence mimicked that seen in VLUs, examination of the biopsies as a whole indicated that there was an altered distribution. The clear zone of elastin loss extending all the way from the papillary into the reticular dermis of the VLU was not present in the DFU (Figure 3A and 3B). Instead, in the DFU, small elastin pockets were found within the upper dermis, the frequency and size of which increased with depth from the epidermal layer.

VvG staining showed that elastin was very limited both within the upper and lower dermal compartments of DFU (Figure 3B). The degree of elastin loss varied but consistently corresponded to the level of collagen loss. The elastin was almost completely absent in the upper and lower dermis (Figure 3B) along with weak collagen staining and thin fibrils.

Herovici staining revealed that, overall, the abundance of collagen type I exceeded that of type III (Figure 3C). However, the presence of type I collagen was severely decreased, with fibril organisation resembling that found in the upper dermis of VLUs (Figure 2). The staining intensity in the reticular dermis was similar to that intact leg tissue but could easily be distinguished because it completely lacked the fibre bundle thickness of intact normal skin.

Taken together, these results show a reduction in the levels of both collagen and elastin throughout the entire dermis in the intact WE skin biopsies of DFUs. Whilst their signals could be detected, it was only in the form of fine wispy fibres and not the thick collagen and elastin bundles seen in normal intact skin.

Immune response – VLU

Cluster of differentiation 68 (CD68) is a general monocyte/macrophage marker (27), whilst CD18 labels integrin beta-2 localised to the surface of a variety of immune cells other than monocytes and macrophages. There was a significant ($P < 0{\cdot}001$) elevation of 5–10-fold in the number of CD68 cells in the dermis of the VLUs compared to intact arm tissue within the upper dermis (Figure 4A–4C). The largest infiltration was seen at the WE with an eightfold elevation in positive cell counts ($P < 0{\cdot}001$), with a steady decline from there to fivefold at 1 mm ($P < 0{\cdot}001$) and threefold at the far edge (FE) ($P = 0{\cdot}03$).

A noticeable increase in CD18-positive cells was found in the upper dermis (Figure 4D–4F), and the number of CD18 positive cells decreased with distance from the WE. This equated to an average sevenfold significant increase ($P < 0{\cdot}001$) in CD18 abundance, which declined to fivefold at the FE ($P = 0{\cdot}018$) location (Figure 4F).

Immune response – DFUs

There was an overall increase in CD68-positive cells in DFUs compared to arm tissue (Figure 5A–5C). There was a 13-fold increase within the WE ($P = 0{\cdot}024$), but the other locations did not reach significance. The number of CD18-positive leukocytes was elevated within the dermis, although the numbers were quite varied. At 1 mm from the WE, there was a 5·3-fold increase ($P = 0{\cdot}022$), although on average a significant change was not identified at the two other dermal ulcer locations (Figure 5F).

Discussion

Second harmonic generation

Second harmonic generation is a non-linear optical phenomenon that takes place when two photons of light interact with one another, where they are annihilated to generate a single photon at half the wavelength. This only takes place in tissues with first-order non-linear susceptibility, which in biological material is found in structures that are birefringent and have a non-centrosymetric crystalline structure, such as fibrillar collagen I and III and actin (25). Using a 2-photon microscope to deliver pulses of light to tissues that are rich in fibrilar collagen, such as the dermis, allows the effective SHG visualisation of unstained collagen bundles. Autofluorescense signals can also be generated from collagen and elastin fibres outside the SHG spectrum, which is very narrow, being half the pump laser's wavelength. SUM of the two signals allows

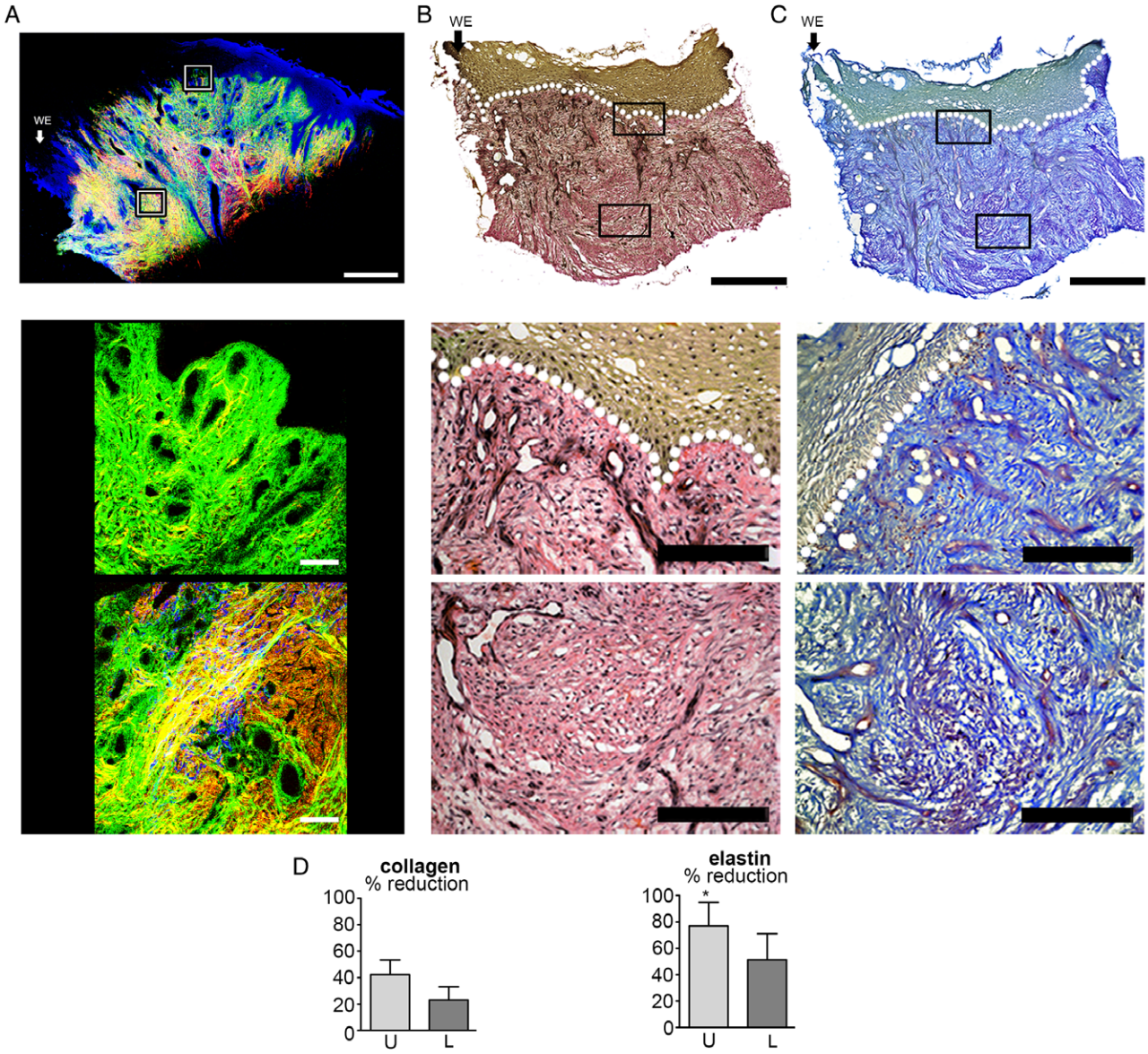

Figure 3 Imaging of the extracellular matrix of diabetic foot ulcer biopsies. (A) Second harmonic generation and autofluorescence imaging of collagen (green, backscatter; red, forward detection) and elastin fibres and nuclei (blue) in a diabetic foot ulcer. Montage of high-power SHG and autofluorescence images of a 4-mm skin biopsy from the edge of a diabetic foot ulcer. High-power images of the upper and lower dermis. (B) Verhoeff van Gieson (VvG) staining collagen red and elastin black in a sister section. Montage followed by high-power images of the upper and lower dermis. (C) Herovici staining differentiates between collagen type I, stained purple, and type III, blue. (D) Graphs quantifying SHG images and the % reduction in signal from collagen and elastin. Arrow and WE marks wound edge to the left of the image. Error bars: mean ± SEM. Scale bars, montage 1 mm and high power 200 µm.

both ECM components, collagen and elastin to be visualised at the same time in unstained tissues. As we see here, the signals we generate in skin are very similar to those of more conventional histological stains. The advantage of the SHG imaging technique is that it does not require staining and can be performed on intact tissues. The use of long wavelengths of light in the infrared range gives good depth penetration and low scattering of the signal. At the same time, this low-energy light is not toxic, and the SHG imaging does not generate any heat and thus is favourable for live cell and tissue imaging. In intact biopsies of pigmented human skin samples, we have been able to image to a depth of 300 µm in the backscattered mode and over 1000 µm in the transmitted mode (26). Given the recent development of more portable multi-photon imaging devices (28,29), this approach may prove useful in the study of the dynamics of these ECM components and give a readout on the breakdown of the collagen ECM away from the WE.

ECM degradation in VLUs and DFUs

The reduced integrity of the dermal ECM of chronic WE tissue can be attributed to a combination of limited component synthesis and maturation along with enhanced degradation. A variety of factors have been attributed to degradation, mainly persistent

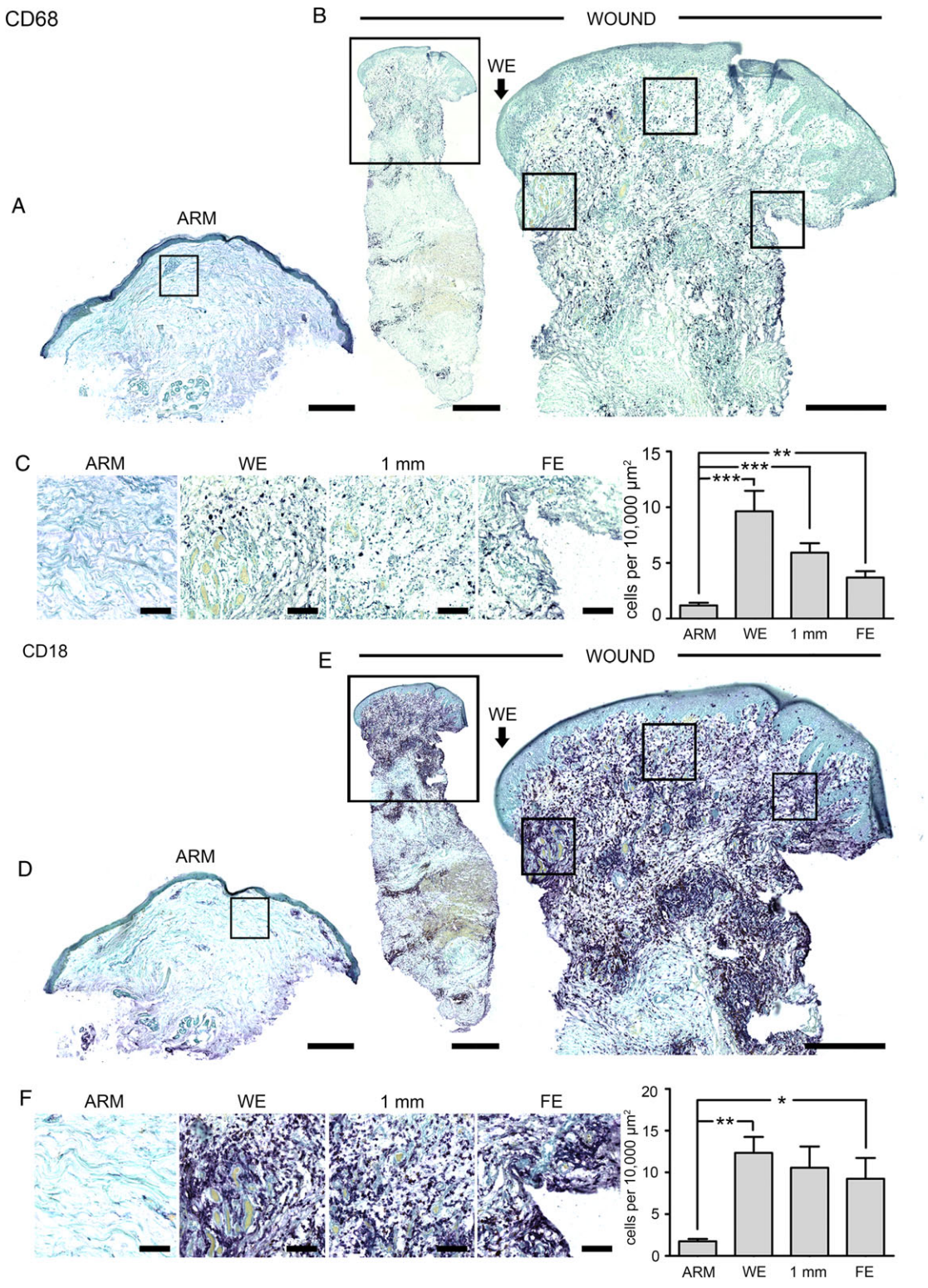

Figure 4 Staining of CD68 and CD18 inflammatory cells in normal skin and venous leg ulcer biopsies. (A) Montage of a section from a 4-mm biopsy from normal arm skin and (B) the edge of a venous leg ulcer stained for CD68 (purple). (C) Higher-power images taken in the upper dermis at the wound edge (WE) 1 mm in and at the far edge (FE). Graphs showing counts of CD68-positive cells demonstrated a significant ($P < 0{\cdot}001$ WE & 1 mm and FE $P < 0{\cdot}01$) elevation compared to normal skin biopsies. (D) Montage of a section from a 4-mm biopsy from normal arm skin and (E) the edge of a venous leg ulcer stained for CD18 (purple). (F) Higher-power images taken in the upper dermis at the wound edge (WE) 1 mm in and at the far edge (FE). (H) Graphs showing counts of CD18-positive cells demonstrated a significant ($P < 0{\cdot}01$ WE, $P < 0{\cdot}05$ FE) elevation compared to normal skin biopsies. Error bars: mean ± SEM. Arrow and WE mark the wound edge. Scale bars, montage 500 µm and high power 100 µm.

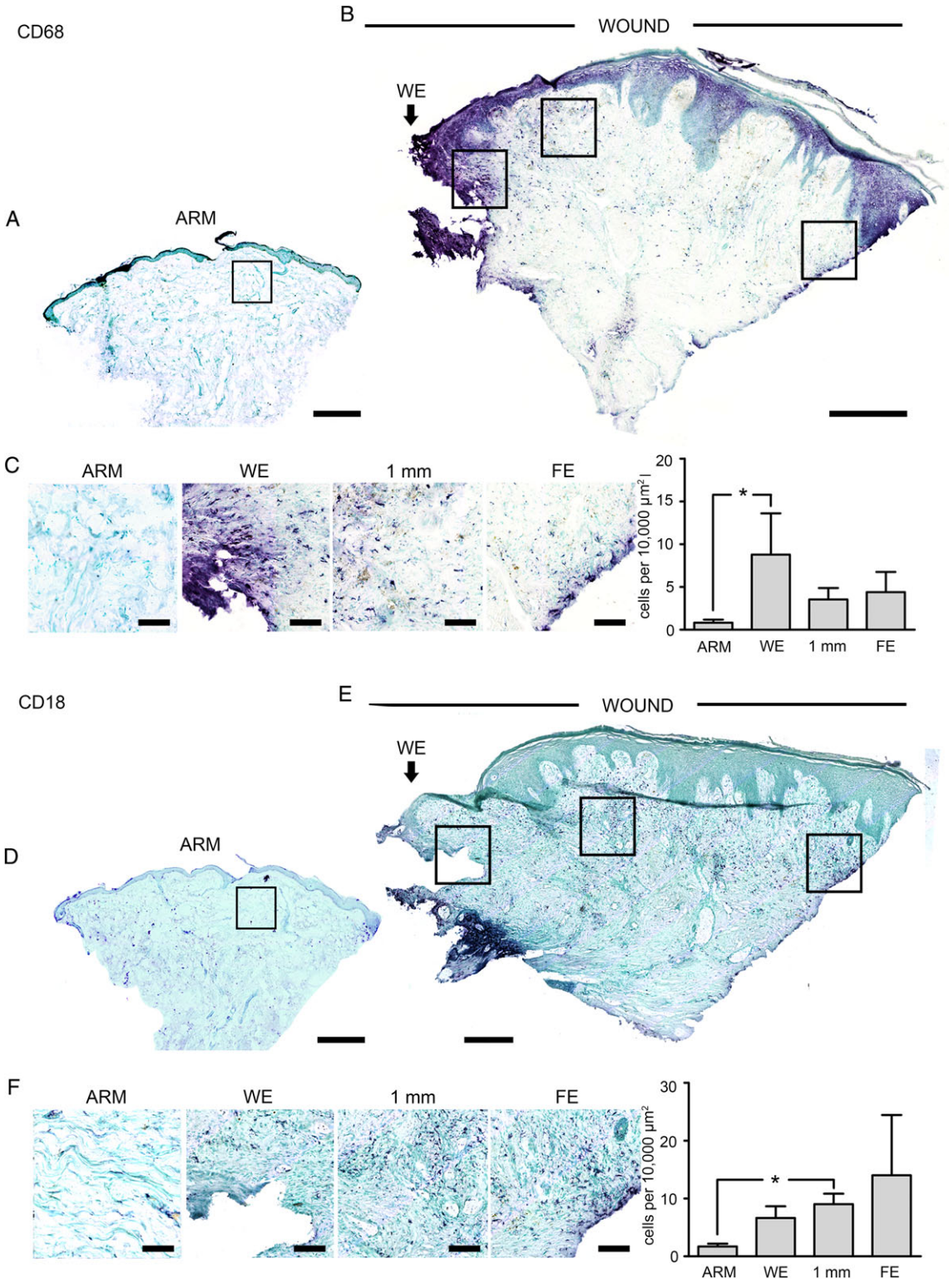

Figure 5 Staining of CD68 and CD18 inflammatory cells in normal skin and diabetic foot ulcer biopsies. (A) Montage of a section from a 4-mm biopsy from normal arm skin and (B) the edge of a diabetic foot ulcer stained for CD68 (purple). (C) Higher-power images taken in the upper dermis at the wound edge (WE) 1 mm in and at the far edge (FE). Graphs of counts of CD68-positive cells showed a significant ($P < 0{\cdot}05$ WE) elevation compared to normal skin biopsies. (D) Montage of a section from a 4-mm biopsy from normal arm skin and (E) the edge of a diabetic foot ulcer stained for CD18 (purple). (F) Higher-power images taken in the upper dermis at the wound edge (WE) 1 mm in and at the far edge (FE). Graphs of counts of CD18-positive cells showed a significant ($P < 0{\cdot}05$ 1 mm) elevation compared to normal skin biopsies. Error bars: mean ± SEM. Arrow and WE mark the wound edge. Scale bars, montage 500 µm and high power 100 µm.

inflammation. This is predominantly self-perpetuating but can be exacerbated by bacterial infection. A persistent immune response, as illustrated by the elevated CD68 and CD18 levels in areas of ECM degradation in both VLUs and DFUs, directly enhances wound protease levels, degrading both collagen and elastin (30). The appearance of senescent fibroblasts, with enhanced ECM degradation, in the WE tissues will also contribute to its destruction (20,22). In addition, collagen synthesis may be limited as a result of elevated dermal fibroblast C × 43 expression (24). This directly reduces pro-collagen synthesis and indirectly reduces fibroblast migration into the wound bed (31,32). Also, collagen maturation is severely inhibited in hypoxic environments, a state frequently identified in chronic wound tissue.

Another consideration is that the cycles of ischaemia–reperfusion are implicated in the continuation of all chronic wound types (3). The re-oxygenation of the tissue, post-hypoxia, is characterised by severe oxidative stress. The subsequent inflammatory cell influx can precipitate repeated oxidative bursts, leading to further damage and perpetuating the wound in a non-healing state.

Mediators of collagen degradation

Dermal integrity loss is primarily a result of an imbalance in matrix metalloproteinase (MMP) and tissue inhibitor of metalloproteinase (TIMP) production. With the reduced oxygen levels that are found in these chronic wounds, MMP production is elevated. These are produced more specifically by fibroblasts (MMP-2) and neutrophils (MMP-9), which can be identified in wound exudates (9). These two proteases specifically target type I collagen and do not degrade type III. Overall, the dominance of collagen type III seen in the upper and lower dermis of many of the VLUs and across the entire dermis of DFUs may be attributed to a lower concentration of the type III collagen-degrading enzymes such as MMP-3 and MMP-10, which have been shown to be at similar levels in acute and chronic wounds (33). Persistently high levels of MMPs in chronic wounds have a negative effect on the healing process, and there is evidence to suggest that protease inhibitors can have beneficial effects on healing (15–17).

Enhanced MMP production may be partially attributed to the fibroblast cell cycle states, which are often senescent within the chronic wound environment (20,22). Pro-collagenase expression has been shown to be constantly elevated in cultured senescent fibroblasts, with a corresponding decrease in TIMP production when compared to young cells (34). The degradation problem is further worsened by insufficient mature collagen deposition. The degree of procollagenhydroxylation at proline and lisine residues is limited by the enzymatic ability of prolyl hydroxylase in enviroments of low oxygen tension, which are common in chronic wounds (35).

Elastin loss may be a direct result of inflammatory stasis in chronic wounds. Neutrophils produce elastase (36) and macrophages metalloelastase (MMP-12) (37) that degrade the elastic fibres. As a result of damage, the level of solubilised elastin increases, in turn stimulating MMP-12 expression by resident dermal fibroblasts (38). In addition, cathepsin G, which is found in high concentration in neutrophils, is capable of degrading intact elastin fibres (39). However, neutrophil elastase may be more integral to elastin hydrolysis, which stimulates MMP-2 (40) and -3 (41) expression by dermal fibroblasts.

Macrophage abundance was most concentrated within the upper dermis of both wound types, where ECM degradation was the highest. Although not quantified, the number of macrophages declined with dermal depth, with minimal detection in the bottom half of the lower dermis and almost a complete absence from the deep regions of VLUs. The leukocyte distribution matched the pattern of elastin loss in both wound types, with fibril abundance increasing with dermal depth.

Excessive elastin loss that extends into tissue within the dermal layer may encourage an increase in wound size due to the loss in tissue elasticity and resilience, particularly over points of stress that is, the heel of the foot, common sites of DFU formation. We can gain some insights from animal models because during murine acute wound healing, tropoelastin and elastin soluble non-cross-linked fibril deposition is seen at 7 days post-wounding, after complete wound closure (42). Without complete reepithelialisation, the signalling molecules required to stimulate elastin expression may not be produced. In the chronic wound environment, this would result in continued elastin loss with minimal replacement. Secreted tropoelastin monomers are tethered to and self-aggregate on the secretory cell surface. If de novo elastin production does occur, mature fibril formation may still be inhibited.

Bacterial contamination

All chronic wounds are colonised by bacteria to some extent, but clinical infection that delays healing is defined as ≥ 10 planktonic colony-forming units (CFU) per gram of tissue (43). Interestingly, impaired repair is still identified in wounds that are not classically deemed infected. In many of these instances, biofilms are present as an accumulation of bacteria enclosed in a self-produced extracellular polymeric matrix. The formation of a biofilm is ×10 more likely in chronic versus acute wounds. Both planktonic infections and biofilm production have been shown to negatively impact wound repair (22). Repeated infections can contribute to the continuation of inflammation beyond initial innate immunity, not allowing inflammation to resolve (44). The altered protease environment instigated by persistent inflammation could be attributed to biofilm contamination, where neutrophils are attracted to the wound site, at which point they degranulate and release ECM-damaging proteolytic enzymes and pro-inflammatory signals (45). Although none of the biopsies were taken from clinically infected wounds, all wounds would have been colonised to some degree at some point, and this may have contributed to the ECM degradation observed in the VLU and DFU samples.

The lack of a normal ECM in the tissue surrounding chronic wounds may itself contribute to poor healing. The ECM and matricellular proteins that bind to it are able to have positive and negative effects on the healing process (46). The group of matricellular proteins, such as vitronectin, osteopontin, thrombospondins, tenascins and galectins, have multiple direct effects on diverse cell types involved in the wound-healing process, and their disruption is likely to have negative effects on healing (46). The presence of normal ECM, not just collagen and

elastin but also glycosaminoglycans, glycoproteins and proteoglycans, regulates many events in the wound-healing process, such as cell migration, proliferation and cells mortality (47), so their degradation is likely to have profound effects on the healing process.

In conclusion, we find broad agreement between the results from conventional histological staining techniques and those from the SHG imaging of collagen fibres and the autofluorescence of elastin fibres. The degradation of the ECM was distinctive between VLUs and DFUs. The DFUs tended to lose elastin and collagen bundles throughout the depth of the dermis, whereas VLUs lost these components in the upper third of the dermis. The loss of collagen and elastin fibres is likely to be due to the persistent inflammation and the senescent fibroblasts found in these chronic wounds combined with poor vasculature and oxygenation that would be required to effectively lay down new ECM. Reducing inflammation and improving the vasculature is clearly required to promote the healing of these chronic wounds. However, identifying a healing or non-healing wound is important. The suggestion that having more than 15% of fibroblasts in a state of senescence will compromise healing could be measured by biopsy (22,23). However, it may be possible to measure their degrading effect on the ECM as a read out of their number or activity and thereby ability to heal (19). Second harmonic imaging of skin at the edge of a chronic wound in a patient may provide useful information for vascular surgeons on both the state of healing (or not) of the wound and the distance from the WE to normal intact tissue during the planning of debridement procedures. Such hand-held SHG imaging devices are now in production (28,29) and will be commercially available very soon. This approach could be very helpful in diagnosing the state of the wound and indicating if intervention is required without taking a biopsy.

References

1. Eming SA, Martin P, Tomic-Canic M. Wound repair and regeneration: mechanisms, signaling, and translation. *Sci Transl Med* 2014;**6**:265sr6.
2. Martin P. Wound healing--aiming for perfect skin regeneration. *Science* 1997;**276**:75–81.
3. Mustoe T. Understanding chronic wounds: a unifying hypothesis on their pathogenesis and implications for therapy. *Am J Surg* 2004;**187**(5A):65S–70.
4. Nunan R, Harding KG, Martin P. Clinical challenges of chronic wounds: searching for an optimal animal model to recapitulate their complexity. *Dis Model Mech* 2014;**7**:1205–13.
5. Martin P, Leibovich SJ. Inflammatory cells during wound repair: the good, the bad and the ugly. *Trends Cell Biol* 2005;**15**:599–607.
6. Sen CK, Gordillo GM, Roy S, Kirsner R, Lambert L, Hunt TK, Gottrup F, Gurtner GC, Longaker MT. Human skin wounds: a major and snowballing threat to public health and the economy. *Wound Repair Regen* 2009;**17**:763–71.
7. Roth RS, Lowery JC, Hamill JB. Assessing persistent pain and its relation to affective distress, depressive symptoms, and pain catastrophizing in patients with chronic wounds: a pilot study. *Am J Phys Med Rehabil* 2004;**83**:827–34.
8. Armstrong DG, Wrobel J, Robbins JM. Guest editorial: are diabetes-related wounds and amputations worse than cancer? *Int Wound J* 2007;**4**:286–7.
9. Wysocki AB, Staiano-Coico L, Grinnell F. Wound fluid from chronic leg ulcers contains elevated levels of metalloproteinases MMP-2 and MMP-9. *J Invest Dermatol* 1993;**101**:64–8.
10. Gill SE, Parks WC. Metalloproteinases and their inhibitors: regulators of wound healing. *Int J Biochem Cell Biol* 2008;**40**:1334–47.
11. Palolahti M, Lauharanta J, Stephens RW, Kuusela P, Vaheri A. Proteolytic activity in leg ulcer exudate. *Exp Dermatol* 1993;**2**:29–37.
12. Trengove NJ, Stacey MC, MacAuley S, Bennett N, Gibson J, Burslem F, Murphy G, Schultz G. Analysis of the acute and chronic wound environments: the role of proteases and their inhibitors. *Wound Repair Regen* 1999;**7**:442–52.
13. Wysocki AB, Grinnell F. Fibronectin profiles in normal and chronic wound fluid. *Lab Invest* 1990;**63**:825–31.
14. McQuibban GA, Butler GS, Gong JH, Bendall L, Power C, Clark-Lewis I, Overall CM. Matrix metalloproteinase activity inactivates the CXC chemokine stromal cell-derived factor-1. *J Biol Chem* 2001;**276**:43503–8.
15. Rayment EA, Dargaville TR, Shooter GK, George GA, Upton Z. Attenuation of protease activity in chronic wound fluid with bisphosphonate-functionalised hydrogels. *Biomaterials* 2008;**29**:1785–95.
16. Eming S, Smola H, Hartmann B, Malchau G, Wegner R, Krieg T, Smola-Hess S. The inhibition of matrix metalloproteinase activity in chronic wounds by a polyacrylate superabsorber. *Biomaterials* 2008;**29**:2932–40.
17. Lobmann R, Zemlin C, Motzkau M, Reschke K, Lehnert H. Expression of matrix metalloproteinases and growth factors in diabetic foot wounds treated with a protease absorbent dressing. *J Diabetes Complications* 2006;**20**:329–35.
18. Mirza RE, Fang MM, Weinheimer-Haus EM, Ennis WJ, Koh TJ. Sustained inflammasome activity in macrophages impairs wound healing in type 2 diabetic humans and mice. *Diabetes* 2014;**63**:1103–14.
19. Herrick SE, Ireland GW, Simon D, McCollum CN, Ferguson MW. Venous ulcer fibroblasts compared with normal fibroblasts show differences in collagen but not fibronectin production under both normal and hypoxic conditions. *J Invest Dermatol* 1996;**106**:187–93.
20. Telgenhoff D, Shroot B. Cellular senescence mechanisms in chronic wound healing. *Cell Death Differ* 2005;**12**:695–8.
21. Mendez MV, Stanley A, Park HY, Shon K, Phillips T, Menzoian JO. Fibroblasts cultured from venous ulcers display cellular characteristics of senescence. *J Vasc Surg* 1998;**28**:876–83.
22. Harding KG, Moore K, Phillips TJ. Wound chronicity and fibroblast senescence--implications for treatment. *Int Wound J* 2005;**2**:364–8.
23. Stanley A, Osler T. Senescence and the healing rates of venous ulcers. *J Vasc Surg* 2001;**33**:1206–11.
24. Sutcliffe JE, Chin KY, Thrasivoulou C, Serena TE, O'Neil S, Hu R, White AM, Madden L, Richards T, Phillips AR, Becker DL. Abnormal connexin expression in human chronic wounds. *Br J Dermatol* 2015;**173**:1205–15.
25. Theodossiou TA, Thrasivoulou C, Ekwobi C, Becker DL. Second harmonic generation confocal microscopy of collagen type I from rat tendon cryosections. *Biophys J* 2006;**91**:4665–77.
26. Thrasivoulou C, Virich G, Krenacs T, Korom I, Becker DL. Optical delineation of human malignant melanoma using second harmonic imaging of collagen. *Biomed Opt Express* 2011;**2**:1282–95.
27. Holness CL, Simmons DL. Molecular cloning of CD68, a human macrophage marker related to lysosomal glycoproteins. *Blood* 1993;**81**:1607–13.
28. Zhao Y, Sheng M, Huang L, Tang S. Design of a fiber-optic multiphoton microscopy handheld probe. *Biomed Opt Express* 2016;**7**:3425–37.
29. Huland DM, Brown CM, Howard SS, Ouzounov DG, Pavlova I, Wang K, Rivera DR, Webb WW, Xu C. In vivo imaging of unstained tissues using long gradient index lens multiphoton endoscopic systems. *Biomed Opt Express* 2012;**3**:1077–85.
30. McDaniel JC, Roy S, Wilgus TA. Neutrophil activity in chronic venous leg ulcers--a target for therapy? *Wound Repair Regen* 2013;**21**:339–51.
31. Mori R, Power KT, Wang CM, Martin P, Becker DL. Acute downregulation of connexin43 at wound sites leads to a reduced inflammatory response, enhanced keratinocyte proliferation and wound fibroblast migration. *J Cell Sci* 2006;**119**(Pt 24):5193–203.

32. Mendoza-Naranjo A, Cormie P, Serrano AE, Wang CM, Thrasivoulou C, Sutcliffe JE, Gilmartin DJ, Tsui J, Serena TE, Phillips AR, Becker DL. Overexpression of the gap junction protein Cx43 as found in diabetic foot ulcers can retard fibroblast migration. *Cell Biol Int* 2012;**36**:661–7.
33. Saarialho-Kere UK. Patterns of matrix metalloproteinase and TIMP expression in chronic ulcers. *Arch Dermatol Res* 1998;**290**(Suppl):S47–54.
34. West MD, Pereira-Smith OM, Smith JR. Replicative senescence of human skin fibroblasts correlates with a loss of regulation and overexpression of collagenase activity. *Exp Cell Res* 1989;**184**:138–47.
35. Hopf HW, Humphrey LM, Puzziferri N, West JM, Attinger CE, Hunt TK. Adjuncts to preparing wounds for closure: hyperbaric oxygen, growth factors, skin substitutes, negative pressure wound therapy (vacuum-assisted closure). *Foot Ankle Clin* 2001;**6**:661–82.
36. Watanabe H, Hattori S, Katsuda S, Nakanishi I, Nagai Y. Human neutrophil elastase: degradation of basement membrane components and immunolocalization in the tissue. *J Biochem* 1990;**108**:753–9.
37. Gronski TJ Jr, Martin RL, Kobayashi DK, Walsh BC, Holman MC, Huber M, Van Wart HE, Shapiro SD. Hydrolysis of a broad spectrum of extracellular matrix proteins by human macrophage elastase. *J Biol Chem* 1997;**272**:12189–94.
38. Almine JF, Wise SG, Hiob M, Singh NK, Tiwari KK, Vali S, Abbasi T, Weiss AS. Elastin sequences trigger transient proinflammatory responses by human dermal fibroblasts. *FASEB J* 2013;**27**:3455–65.
39. Schmelzer CE, Jung MC, Wohlrab J, Neubert RH, Heinz A. Does human leukocyte elastase degrade intact skin elastin? *FEBS J* 2012;**279**:4191–200.
40. Huet E, Brassart B, Wallach J, Debelle L, Haye B, Emonard H, Hornebeck W. Effect of elastin peptides on the production of matrix metalloproteinase 2 by human skin fibroblasts in culture. *J Soc Biol* 2001;**195**:165–72.
41. Brassart B, Fuchs P, Huet E, Alix AJ, Wallach J, Tamburro AM, Delacoux F, Haye B, Emonard H, Hornebeck W, Debelle L. Conformational dependence of collagenase (matrix metalloproteinase-1) up-regulation by elastin peptides in cultured fibroblasts. *J Biol Chem* 2001;**276**:5222–7.
42. Shuttleworth L, Black RA, Ferguson MWJ, Herrick SE. Deposition of elastic fibres in a murine cutaneous wound healing model. *Eur Cells Mater* 2005;**10**(SUPPL.2):18.
43. Percival SL, Thomas JG, Williams DW. Biofilms and bacterial imbalances in chronic wounds: anti-Koch. *Int Wound J* 2010;**7**:169–75.
44. Secor PR, James GA, Fleckman P, Olerud JE, McInnerney K, Stewart PS. Staphylococcus aureus biofilm and planktonic cultures differentially impact gene expression, mapk phosphorylation, and cytokine production in human keratinocytes. *BMC Microbiol* 2011; **11**:143.
45. Meyle E, Stroh P, Gunther F, Hoppy-Tichy T, Wagner C, Hansch GM. Destruction of bacterial biofilms by polymorphonuclear neutrophils: relative contribution of phagocytosis, DNA release, and degranulation. *Int J Artif Organs* 2010;**33**:608–20.
46. Midwood KS, Williams LV, Schwarzbauer JE. Tissue repair and the dynamics of the extracellular matrix. *Int J Biochem Cell Biol* 2004;**36**:1031–7.
47. Maquart FX, Monboisse JC. Extracellular matrix and wound healing. *Pathol Biol* 2014;**62**:91–5.